Research Article | Vol. 24, No. 14 | 11 Jul 2016 | OPTICS EXPRESS 16156

Optics EXPRESS

Two-photon luminescence thermometry: towards 3D high-resolution thermal imaging of waveguides

RUIYUN HE,[1,2] JAVIER RODRÍGUEZ VÁZQUEZ DE ALDANA,[3] GINÉS LIFANTE PEDROLA,[2] FENG CHEN,[1,4] AND DANIEL JAQUE[2,5]

[1]*School of Physics, State Key Laboratory of Crystal, Shandong University, Jinan 250100, China*
[2]*Fluorescence Imaging Group, Departamento de Física de Materiales, Facultad de Ciencias, Universidad Autónoma de Madrid, Madrid 28049, Spain*
[3]*Aplicaciones del Láser y Fotónica (ALF-USAL), Universidad de Salamanca, Salamanca 37008, Spain*
[4]*drfchen@sdu.edu.cn*
[5]*daniel.jaque@uam.es*

Abstract: We report on the use of the Erbium-based luminescence thermometry to realize high resolution, three dimensional thermal imaging of optical waveguides. Proof of concept is demonstrated in a 980-nm laser pumped ultrafast laser inscribed waveguide in Er:Yb phosphate glass. Multi-photon microscopy images revealed the existence of well confined intra-waveguide temperature increments as large as 200 °C for moderate 980-nm pump powers of 120 mW. Numerical simulations and experimental data reveal that thermal loading can be substantially reduced if pump events are separated more than the characteristic thermal time that for the waveguides investigated is in the ms time scale.

OCIS codes: (110.6820) Thermal imaging; (300.6410) Spectroscopy, multiphoton; (160.5690) Rare-earth-doped materials; (130.2755) Glass waveguides.

References and Links

1. G. Lifante, *Integrated Photonics: Fundamentals* (JohnWiley and Sons, 2008).
2. T. Suhara and M. Fujimura, *Waveguide Nonlinear-Optic Devices* (Springer, 2003).
3. A. J. Glass and A. H. Guenther, "Laser induced damage of optical elements–a status report," Appl. Opt. **12**(4), 637–649 (1973).
4. W. Koechner, "Thermal lensing in a Nd:YAG laser rod," Appl. Opt. **9**(11), 2548–2553 (1970).
5. M. B. Bavil and E. Safari, "Thermal and stress analyses in an end-pumped Nd:YAG slab laser using finite element method," J. Mech. Sci. Technol. **28**(8), 3231–3236 (2014).
6. G. Schreiber, H. Suche, Y. L. Lee, W. Grundkötter, V. Quiring, R. Ricken, and W. Sohler, "Efficient cascaded difference frequency conversion in periodically poled Ti:$LiNbO_3$ waveguides using pulsed and cw pumping," Appl. Phys. B **73**(5), 501–504 (2014).
7. D. Jaque and F. Vetrone, "Luminescence nanothermometry," Nanoscale **4**(15), 4301–4326 (2012).
8. C. D. S. Brites, P. P. Lima, N. J. O. Silva, A. Millán, V. S. Amaral, F. Palacio, and L. D. Carlos, "Thermometry at the nanoscale," Nanoscale **4**(16), 4799–4829 (2012).
9. R. He, J. R. Vázquez de Aldana, G. L. Pedrola, F. Chen, and D. Jaque, "All-optical thermal microscopy of laser-excited waveguides," Opt. Lett. **41**(9), 2061–2064 (2016).
10. F. Vetrone, R. Naccache, A. Zamarrón, A. Juarranz de la Fuente, F. Sanz-Rodríguez, L. Martinez Maestro, E. Martín Rodriguez, D. Jaque, J. García Solé, and J. A. Capobianco, "Temperature sensing using fluorescent nanothermometers," ACS Nano **4**(6), 3254–3258 (2010).
11. S. F. León-Luis, U. R. Rodríguez-Mendoza, I. R. Martín, E. Lalla, and V. Lavín, "Effects of Er^{3+} concentration on thermal sensitivity in optical temperature fluorotellurite glass sensors," Sens. Actuators B Chem. **176**, 156–164 (2013).
12. P. Haro-González, B. del Rosal, L. M. Maestro, E. M. Rodríguez, R. Naccache, J. A. Capobianco, K. Dholakia, J. G. Solé, and D. Jaque, "Optical trapping of $NaYF_4$:Er^{3+},Yb^{3+} upconverting fluorescent nanoparticles," Nanoscale **5**(24), 12192–12199 (2013).
13. P. Du, L. Luo, W. Li, and Q. Yue, "Upconversion emission in Er-doped and Er/Yb-codoped ferroelectric $Na_{0.5}Bi_{0.5}TiO_3$ and its temperature sensing application," J. Appl. Phys. **116**(1), 014102 (2014).
14. S. A. Wade, S. F. Collins, and G. W. Baxter, "Fluorescence intensity ratio technique for optical fiber point temperature sensing," J. Appl. Phys. **94**(8), 4743–4756 (2003).
15. K. T. V. Grattan and T. Sun, "Fiber optic sensor technology: an overview," Sensor. Actuat. A-Phys. **82**, 40–61 (2000).

#267158 http://dx.doi.org/10.1364/OE.24.016156
Journal © 2016 Received 26 May 2016; revised 2 Jul 2016; accepted 2 Jul 2016; published 8 Jul 2016

Optics EXPRESS

16. F. Chen and J. R. V. de Aldana, "Optical waveguides in crystalline dielectric materials produced by femtosecond-laser micromachining," Laser Photonics Rev. **8**(2), 251–275 (2014).
17. S. Gross and M. J. Withford, "Ultrafast-laser-inscribed 3D integrated photonics: challenges and emerging applications," Nanophotonics **4**(3), 332–352 (2015).
18. K. Sugioka and Y. Cheng, "Ultrafast lasers—reliable tools for advanced materials processing," Light Sci. Appl. **3**(4), e149 (2014).
19. V. K. Rai, "Temperature sensors and optical sensors," Appl. Phys. B **88**(2), 297–303 (2007).
20. L. Marciniak, K. Waszniewska, A. Bednarkiewicz, D. Hreniak, and W. Strek, "Sensitivity of a nanocrystalline luminescent thermometer in high and low excitation density regimes," J. Phys. Chem. C **120**(16), 8877–8882 (2016).
21. Z. Cai, A. Chardon, H. Xu, P. Féron, and G. M. Stéphan, "Laser characteristics at 1535 nm and thermal effects of an Er:Yb phosphate glass microchip pumped by Ti:sapphire laser," Opt. Commun. **203**(3–6), 301–313 (2002).
22. S. Chénais, S. Forget, F. Druon, F. Balembois, and P. Georges, "Direct and absolute temperature mapping and heat transfer measurements in diode-end-pumped Yb:YAG," Appl. Phys. B **79**(2), 221–224 (2004).
23. J. Petit, B. Viana, and P. Goldner, "Internal temperature measurement of an ytterbium doped material under laser operation," Opt. Express **19**(2), 1138–1146 (2011).
24. G. Canat, J. C. Mollier, Y. Jaouën, and B. Dussardier, "Evidence of thermal effects in a high-power Er^{3+}-Yb^{3+} fiber laser," Opt. Lett. **30**(22), 3030–3032 (2005).
25. A. Kosterin, J. K. Erwin, M. Fallahi, and M. Mansuripur, "Heat and temperature distribution in a cladding-pumped, Er: Yb co-doped phosphate fiber," Rev. Sci. Instrum. **75**(12), 5166–5172 (2004).
26. Y. Z. Xu, H. Y. Tam, S. Y. Liu, and M. S. Demokan, "Pump-Induced thermal effects in Er–Yb fiber grating DBR lasers," IEEE Photonics Technol. Lett. **10**(9), 1253–1255 (1998).
27. T. Liu, Z. M. Yang, and S. H. Xu, "3-Dimensional heat analysis in short-length Er^{3+}/Yb^{3+} co-doped phosphate fiber laser with upconversion," Opt. Express **17**(1), 235–247 (2009).
28. Y. Bellouard, E. Barthel, A. A. Said, M. Dugan, and P. Bado, "Scanning thermal microscopy and Raman analysis of bulk fused silica exposed to low-energy femtosecond laser pulses," Opt. Express **16**(24), 19520–19534 (2008).
29. Y. P. Lan, Y. F. Chen, and S. C. Wang, "Repetition-rate dependence of thermal loading in diode-end-pumped Q-switched lasers: influence of energy-transfer upconversion," Appl. Phys. B **71**(1), 27–31 (2000).
30. S. R. Bowman, S. P. O'Connor, and S. Biswal, "Ytterbium laser with reduced thermal loading," IEEE J. Quantum Electron. **41**(12), 1510–1517 (2005).
31. J. F. Philipps, T. Töpfer, H. Ebendorff-Heidepriem, D. Ehrt, and R. Sauerbre, "Spectroscopic and lasing properties of Er^{3+}:Yb^{3+}-doped fluoride phosphate glasses," Appl. Phys. B **72**(4), 399–405 (2001).
32. B. Lai, L. Feng, J. Wang, and Q. Su, "Optical transition and upconversion luminescence in Er^{3+} doped and Er^{3+}–Yb^{3+} co-doped fluorophosphate glasses," Opt. Mater. **32**(9), 1154–1160 (2010).

1. Introduction

Optical waveguides (WGs) are building blocks in modern integrated photonics as they provide full control over light propagation in the micrometric scale in an analogous way that microwires do in electrical circuits [1]. WGs are based on the controlled refractive index modulation at the micro and sub-micro scales designed for light confinement in an active volume of an enhanced refractive index and/or surrounded by low refractive index media. The requirements of integrated photonics restrict the typical dimensions of active volumes down to a few microns. Under those conditions, large photon densities could be achieved inside WGs and, hence, inside photonic circuits. Such large photon densities could be beneficial for some applications (e.g., those involving nonlinear processes [2]) but could also lead to the appearance of adverse effects [3–5]. Among all of the potential arising adverse effects, local heating has been well known to be of special relevance [3]. Intra-waveguide local heating arises from the partial absorption of propagating light by the material and its subsequent re-emission in the form of heat that could lead to relevant temperature increments at the WG volume and its surroundings. These local light-induced heating could lead to the appearance of a variety of adverse effects. For instance, the optical performance of any optical WG is determined by the refractive index contrast between WG active volume and its surroundings [4]. In most of the cases, refractive index is temperature-dependent so that intra-waveguide heating could modify the refractive index of WG active volume and, the refractive index contrast. This would lead to deterioration in the confinement ability of the optical WGs. In addition, the appearance of relevant thermal gradients in integrated photonic circuits could give place to the creation of no negligible stress fields that could affect both the performance and lifetime of those integrated circuits [5]. Moreover, in waveguide frequency converters

Optics EXPRESS

inscribed in non-linear crystal, the efficient generation of the new wavelength (i.e. second harmonic) is based on phase matching condition, that is very critical with slight changes of temperature. The conversion efficiency is thus highly dependent on temperature [6]. Control over heat generation processes inside WGs therefore becomes essential. Thermal control requires, as a first step, a detailed knowledge of the temperature patterns created by the propagating radiation inside WGs. The acquisition of thermal images of active WGs with sub-micron resolution is not an easy task at all. Thermal imaging of WGs should be obtained in a contact-less mode so that the optical performance of the WG would be non-affected by the measuring performance. Additionally, as WGs are three dimensional (3D) structures, full characterization would require the acquisition of 3D thermal images. Classical methods, such as Scanning Thermal Microscopy or Thermal Lens based interference methods failed to satisfy these two requirements simultaneously. Thus, the development of new thermal imaging techniques should be developed for thermal imaging of integrated optical WGs.

Luminescence Thermometry (LT) [7,8] is a relatively new thermal imaging technique that has been demonstrated to be a simple, flexible and sensitive approach capable of providing contact-free, 3D images of a great variety of systems. LT is based on the extraction of thermal information from an appropriate analysis of fluorescence images. Very recent works have demonstrated the suitability of LT for 3D thermal imaging of optical WGs, in particular of Nd:YAG WGs [9]. In that case, the Neodymium ions were used as thermal probes and the 3D capacity was provided by using a confocal architecture. In these conditions thermal sensitivity of obtained images was limited to 2 °C. To improve the thermal sensitivity of WGs thermal imaging, other luminescence probes with a superior sensitivity is required. Among the different luminescent ions as thermal sensors used in recent years, Erbium ions have been emerged of special relevance as they provide, based on their visible emission bands, thermal sensitivities in a large variety of materials larger than 0.01 $°C^{-1}$ (one order of magnitude larger than those provided, for example, by Neodymium ions) [10,11]. In addition, when combined with appropriate donor ions (such as Ytterbium), the thermal sensitive visible band of Erbium ions can be efficiently excited by infrared (980-nm) via a two-photon excitation process [12,13]. This would provide the LT with a superior spatial resolution via multi-photon microscopy without requiring the use of confocal apertures, i.e. with an improved acquisition times and signal-to-noise ratio. Erbium ions have been used in the past as thermal sensors in fibers [14,15] but its application for the acquisition of high spatial and thermal resolution 3D thermal images of integrated optical WGs has not been explored yet.

In this work, we focus on an Ytterbium and Erbium codoped phosphate glass produced by ultrafast laser inscription (ULI), a well-known technique for waveguide fabrication in dielectrics [16–18], and report on the acquisition of two-photon and 3D thermal images of ULI waveguides (ULI-WGs) by LT. The "pump and probe" experiments in combination with two-photon microscopy have been used to elucidate the 3D spatial extension and magnitude of the 980-nm laser-induced thermal loading in both the WG active volume and surroundings. Time modulation of the 980-nm pump radiation has been used to investigate the dynamics of thermal loading processes inside the WG. Results have been compared to numerical simulations, being in good agreement.

2. Experimental details

The Er:Yb:phosphate glass (doped with 1.5 wt.% Er_2O_3 and 4.5 wt.% Yb_2O_3) used in this work was cut to dimensions of 17 × 9 × 2 mm^3 and with all the faces polished to optical quality. An amplified Ti:Sapphire laser system operating at a wavelength of 800-nm, which produced pulses of 120 fs duration, 1 mJ maximum pulse energy at a repetition rate of 1 kHz, was utilized to fabricate surface cladding structures in the glass sample. For doing so the sample was placed in a 3-axes motorized stage with a spatial resolution better than 100 nm. The laser beam was focused through the sample surface by a 40 × microscope objective (N.A. = 0.65). Pulse energy of 0.36 μJ was found as the optimum value to produce filaments while

Optics EXPRESS

scanning the sample at a constant velocity of 0.5 mm/s. By inscribing parallel filaments with a lateral separation of 3 μm at different depths, surface cladding structures were inscribed.

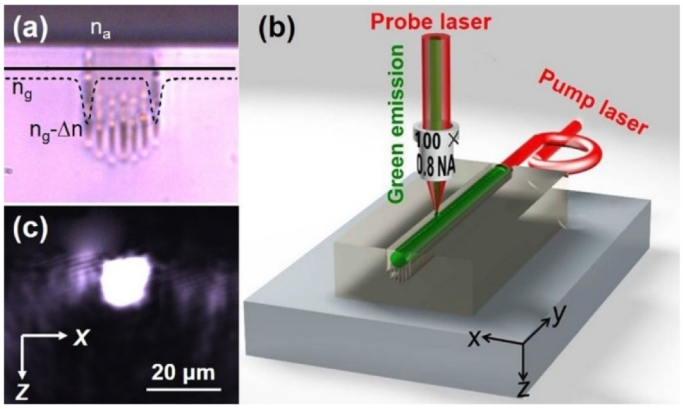

Fig. 1. (a) Cross-sectional optical microscope image of the surface cladding WG. The dashed line illustrate the refractive index profile at the depth of 5 μm, as indicated by the solid line. (b) Schematic of the "pump and probe" experimental setup. (c) Near-field spatial modal distribution at 800-nm. The scale bar is 20 μm for both (a) and (c).

Figure 1(a) shows the cross sectional optical microscope image of the surface cladding WG. The WG consists on a 17 μm in diameter semi-circle constituted by seven filaments and the glass/air interface. The ULI filaments has a decreased refractive index Δn. The waveguide core (n_g) is surrounded by the low refractive index ULI filaments (n_g-Δn) and the air (n_a = 1). The dashed line in Fig. 1(a) illustrates the refractive index profile at the depth of 5 μm, from which the two lateral filaments with low refractive index are clearly shown. These filaments act as a low-index barrier to confine the light propagation inside the waveguide volume. By using an end-coupling arrangement, a single mode fiber was pigtailed into the endface of the WG, as shown in Fig. 1(b). Figure 1(c) shows the near-field spatial modal distribution at 800-nm collected from the opposite endface of the WG, showing well-confined propagation. A schematic plot of the experimental setup used for two-photon florescence measurements and thermal imaging is included in Fig. 1(b). The Er:Yb phosphate glass was mounted on an *XYZ* motorized stage that allows the 3D scanning. The sample was optically excited by means of a single-mode fiber-coupled 980-nm laser diode. The "probe" laser beam was tightly focused into the sample by using a 100 × (NA = 0.80) near-infrared long working distance microscope objective. Based on the parameters of the "probe" laser beam and the microscope objective, the voxel volume of the "probe" laser is estimated to be 2.5 μm^3. The "pump" laser beam was coupled into the waveguide endface by single mode fiber.

The 980-nm laser radiation is absorbed by the Yb^{3+} ions ($^2F_{7/2} \rightarrow {}^2F_{5/2}$ transition), and then the energy is transferred from Yb^{3+} ions to Er^{3+} ions, leading to the excitation of Erbium ions up to $^2H_{11/2}$, and $^4S_{3/2}$ level, from which the subsequent green luminescence is generated, as depicted in Fig. 2(a). The two-photon green luminescence signal was collected by the same microscope objective and spectrally analyzed by a high-resolution spectrometer (Horiba Jobin Yvon iHR320). The micro-luminescence spectrum obtained in our experiment is shown in Fig. 2(b). In this work, we focused on the two thermal sensitive emission lines (525 nm and 545 nm, as depicted in Fig. 2(b)) as they can be used to detect the temperature modifications in the ULI Er:Yb:phosphate glass WGs. As commented in the introduction, several works have revealed that the intensity ration between these two emission lines can be used for high resolution thermal sensing. Such thermal sensitivity arises from the fact that these two lines are originated from the thermally coupled $^2H_{11/2}$ and $^4S_{3/2}$ states. As temperature changes, population redistribution among these states takes place, leading to remarkable change in the intensity ratio between these bands, in such a way that this intensity ratio can be used as a

Optics EXPRESS

temperature indicator. Figure 2(b) includes two micro-luminescence spectra obtained by coupling the 980-nm "pump" laser beam into the WG volume at two different powers, which induce different temperature increments in the WG. The remarkable ratio increment between the two emission lines as the temperature increases is observed. The intensity ratio R between the two visible bands, obtained as a function of the sample temperature, is shown in Fig. 2(c). The emission intensities were measured under only "probe" laser excitation when the glass sample was placed at a heating plate with temperature control from 10 to 60 °C. As can be observed the intensity ratio R varies in a linear way in the temperature range under this study. From the linear fit of experimental data, we can extract a relative ratiometric thermal sensitivity S to be 0.9% °C^{-1}, where S is defined as [19]:

$$S = \frac{1}{R}\frac{dR}{dT} \tag{1}$$

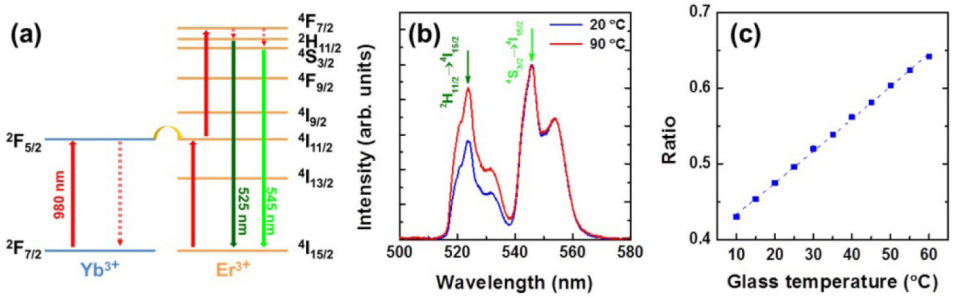

Fig. 2. (a) Energy level diagram showing the relevant states of the Yb^{3+} and Er^{3+} ions and the two-step up conversion excitation mechanism. (b) Normalized micro-luminescence emission spectra obtained at two different "pump" laser powers. The two emission lines used for ratiometric thermal sensing are indicated. (c) Ratio increment as a function of the glass temperature. The dashed line indicates the linear fit of the experimental data.

3. Results and discussion

In the "probe and pump" setup, the "probe" beam is considered as a background contribution. The temperature increment caused by the "probe" beam is estimated to be 40 °C, which is a fixed constant value in the following measurements. To get rid of the fluorescence variation created by the "probe" beam, we have measured the "ratio maps" with the 980-nm "pump" beam "on" or "off", while the "probe" beam is fixed at the same power. The net variation induced by the "pump" beam in the intensity ratio was obtained by subtracting the ratio map with the "pump" beam off and "probe" beam on from that with both the "pump" and "probe" beams on. The temperature increment ΔT refers to thermal loading induced by the "pump" laser propagating in the waveguide with the background temperature is excluded. A recent work on the Er based luminescent thermometer proves that the excitation power density is an important factor to the thermal sensitivity determination [20]. Here we discussed the effect of the excitation power density in our "probe" and "pump" measurement, showing that the thermal sensitive is a constant in this system. For the "probe" laser, the excitation density is estimated to be 2×10^6 W/cm^3, while it is lower by two orders of magnitude for the "pump" laser, ranging from 2×10^4 to 4×10^4 W/cm^3 at different powers. So we can conclude that the variation of the thermal sensitivity at different "pump" laser densities is negligible as the "probe" laser density is much higher. The large ratiometric thermal sensitivity of Erbium ions (Fig. 2(c)) allows us to obtain 3D thermal images from the proper calibration of the 3D micro-luminescence images obtained in terms of the intensity ratio R.

Optics EXPRESS

3.1 Thermal loading under continuous wave excitation

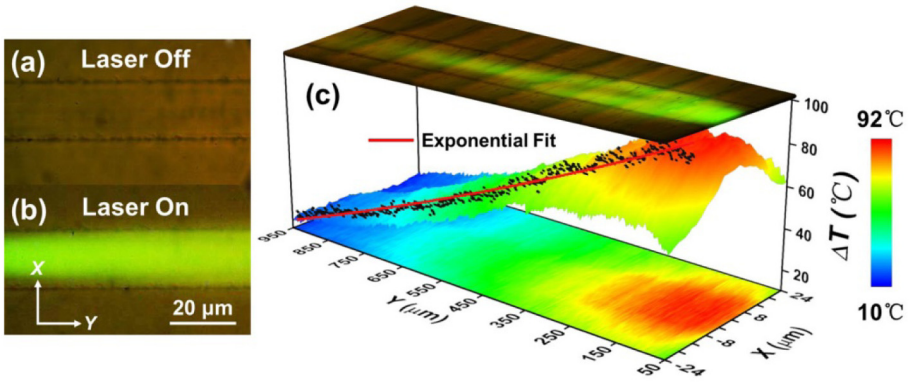

Fig. 3. Microscope images of the WG surface: (a) "pump" laser off and (b) "pump" laser on, in which the confined green emission generated by the "pump" 980-nm laser is clearly shown. (c) 2D temperature image obtained along the WG propagation direction (*Y*). Position *Y* = 0 μm corresponds to the input face of the WG. The horizontal scan path (*X*) is indicated by the solid line in Fig. 1(a). The top view shows the green emission along the WG. The black dots are experimental data extracted from the 2D temperature image, illustrating ΔT versus position along WG propagation direction (*Y*) at *X* = 0 (in the middle of the waveguide volume). The solid red line is the exponential fit of the experimental data.

Following the above explained procedure we firstly obtained the temperature patterns created by the 980-nm "pump" radiation in the *XY* plane (top thermal images). Figures 3(a) and 3(b) depict the microscope top images of the WG. When the 980-nm "pump" laser was switched off, optical image reveal the presence of the parallel ULI damage tracks constituting the WG. On the other hand, in presence of 980-nm "pump" radiation propagating along the WG, the up-converted green emission generated by Erbium ions is clearly observed, being well confined within the WG volume (i.e. between damage tracks). The *XY* (top) thermal image was obtained by scanning the "probe" beam in the *XY* plane at a fixed depth (*Z* = 5 μm) while keeping the "pump" laser power fixed. Figure 3(c) shows the experimentally obtained *XY* image as obtained for a "pump" 980-nm laser power of 60 mW. From this *XY* temperature image, several conclusions can be extracted:

i. The "pump" laser induced intra-waveguide heating decreases along the WG propagation direction *Y*, being mainly concentrated in the first millimeter. This fact is attributed to the strong absorption of the 980-nm "pump" radiation along the WG by the Ytterbium ions. Indeed the absorption coefficient of our Er:Yb codoped phosphate glass has been measured to be α_{abs} = 8.2 cm^{-1} at 980-nm, so that the propagation length of "pump" radiation is expected to be L_{abs} = 1.2 mm, defined as the length at which, the laser power is declined to 1/e of the input power. The absorption of pump radiation during the first 1 mm is further proved by the optical image included in Fig. 3(c) from which it is clear that green emission is almost completely attenuated along the first 1 mm of propagation length. What is more, the temperature increment is plotted as a function of the position along the waveguide propagation direction *Y*, following a good exponential fit.

ii. Secondly, thermal images revealed the presence of laser-induced thermal loadings as large as 92 °C for a moderate 980-nm "pump" power of 60 mW. This fact suggests that pump-induced thermal effects in Er:Yb glass WGs cannot be neglected at all and should be seriously considered during design and operation of such devices. These pump-induced thermal loadings have been, indeed, found to be comparable in a Er:Yb phosphate glass microchip laser [21], and much larger than lasers in Yb doped crystals [22,23] and Er:Yb codoped fibers [24–27].This large pump induced thermal loading could be due to the

Optics EXPRESS

large pump laser densities achieved in our WGs in which 980-nm pump radiation is confined between damage tracks separated only 17 µm.

iii. Finally, although the 980-nm pump radiation is well confined within WG volume, the temperature pattern clearly extends over the surroundings of the WG due to thermal diffusion.

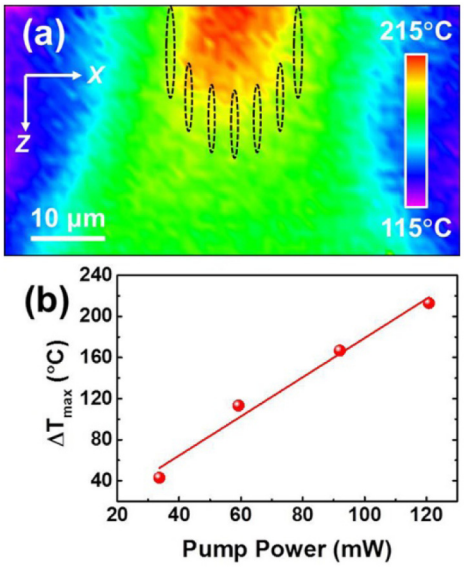

Fig. 4. (a) The cross sectional thermal image obtained at a distance of 50 µm from the input WG face with a CW 980-nm pump laser at a power of 120 mW. Dashed lines indicate the position of damage tracks. (b) Maximum temperature increments induced by different pump powers.

In order to get additional information about the confinement of the pump induced temperature pattern in the WG, we have also measured the cross sectional thermal image of the WG by scanning the 980-nm "probe" spot along the *XZ* plane. Figure 4(a) shows a WG cross sectional thermal image obtained at a distance of 50 µm from the input face with a CW 980-nm pump laser at a power of 120 mW. From this thermal image it is clear that, although some heating is also produced in the surroundings of the WG, it is mostly localized within the WG volume. Indeed, the ULI filaments (indicated by the dashed lines in Fig. 4(a)) seem to be producing an efficient thermal confinement that results in a high temperature increment inside the WG volume, reaching a maximum temperature increment around 215 °C. This suggests that damage filaments could act as "thermal barriers". This behavior is further supported by the fact that the observed "temperature spreading" in the surroundings of WG volume is highly anisotropic. Along the *Z* direction, parallel to the filaments, temperature gradients in the surroundings of WG are found to be close to 1.5 °C/µm whereas along the horizontal *X* direction (perpendicular to damage filaments) thermal gradients increase up to 1.9 °C/µm. These facts indicate that ULI damage filaments are behaving as anisotropic thermal barriers. This is, indeed, in agreement with the results published by Belloudard *et al.* [28] which concluded that ULI damage produced in transparent materials is characterized by a reduced thermal conductivity.

Finally, by measuring thermal images for different "pump" powers we were able to determine the variation of temperature increment induced at WG volume (ΔT_{max}) as a function of the 980-nm "pump" power. Results obtained at a fixed distance (50 µm) from the WG input endface are shown in Fig. 4(b). Note that in the "pump" power range under study in this work, the induced temperature increment has been found to follow a linear trend with

Optics EXPRESS

the 980-nm "pump" power. This fact reveals that, despite the large temperature increments induced in the WG volume (in excess of 200 °C), those are not causing relevant leaking of 980-nm "pump" radiation out of the WG, which would be detected by the appearance of sublinear behaviors in the temperature versus pump power curve.

3.2 Thermal loading under pulse excitation: Thermal accumulation effects

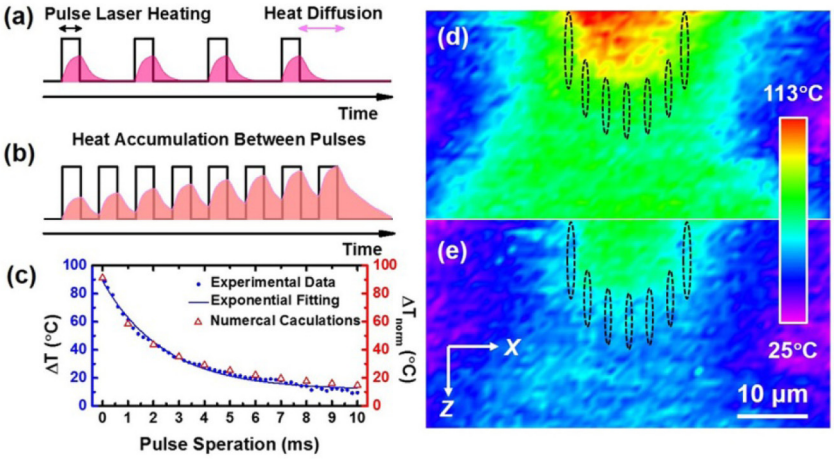

Fig. 5. Schematic representation of the heating and diffusion processes induced by a train of square laser pulses. (a) The pulse separation is long enough that the thermal diffusion has carried the heat away from the sample before the next pulse arrives. (b) The pulse separation is shorter than the time for heat to diffuse away, resulting in an accumulation of heat. (c) The experimental (solid circles) and numerical calculation (triangles) of temperature increment as a function of the pulse separation. The peak power was fixed to 60 mW, and the pulse width was fixed to 2 ms. (d) and (e) show the cross sectional thermal images obtained at a distance of 50 μm from the input face. (d) CW laser with a "pump" power of 60 mW. (e) Square pulse laser with a pulse separation of 2 ms and peak power of 60 mW. Dashed lines indicate the position of damage tracks.

Data included in previous section reveal that 980-nm pump induced thermal loading in Er:Yb ULI glass WGs cannot be neglected at all and it could lead to the appearance of adverse effects that could result, in the long term scale, to severe deterioration in their optical performance. In this sense, new strategies have to be developed to reduce this large thermal loading to avoid undesired deterioration. It has been proposed and experimentally demonstrated in previous works that time modulation of pump radiation could be used for efficient reduction of thermal loading. When the time distance between consecutive pump pulses (i.e., pulse separation) is larger than the characteristic thermal relaxation time ($\tau_{thermal}$), thermal accumulation between consecutive laser pulses is minimized resulting on a reduced average heating [21,26]. This possibility has been demonstrated to be especially suitable for the optimization of the laser performance of microchip lasers that are also characterized by large pump-induced thermal loadings of the active volume [29,30]. Nevertheless, up to the best of our knowledge, this possibility has not been yet demonstrated in laser excited WGs. In this section we have systematically studied the average heating induced in our ULI Er:Yb glass WGs by time-modulated pump radiation. The 980-nm "pump" laser was time-modulated to generate a train of square laser pulses with a fixed pulse width of 2 ms, a peak power of 60 mW and a pulse separation ranging from 0.1 ms to 10 ms. The waveform of the pulse laser is schematically illustrated in Figs. 5(a) and 5(b) for pulse separations significantly larger and shorter than the thermal relaxation time, respectively. In Fig. 5(a), when the pulse separation was significantly larger than $\tau_{thermal}$, almost complete heat dissipation occurs between pump pulses, in such a way that thermal accumulation does not take place. On the

Optics EXPRESS

other hand, when the pulse separation is below $\tau_{thermal}$, thermal relaxation between consecutive pump pulses does not occur and, as a result, thermal accumulation takes place, leading to a larger average temperature increment (Fig. 5(b)). This was experimentally verified by measuring the intra-waveguide temperature increment as a function of the pulse separation. Experimental data are included in Fig. 5(c) as solid circles. The uncertainty of the temperature increment is estimated to be ± 2 °C, showing the high accuracy of the data. It has been observed that the intra-waveguide temperature increment decreases monotonously with the pulse separation. By fitting the temperature increment versus time to a single exponential decay, a characteristic time constant close to 2 ms is found. Thus we conclude that the observed decrease in the average temperature increment is, indeed, caused by a reduction in the thermal accumulation between pump pulses.

The advantage of using time-modulated pump radiation is further evidenced in Figs. 5(d) and 5(e). In these figures we show the cross sectional thermal images obtained when the "pump" beam had a constant power of 60 mW and when the "pump"beam was constituted by a train of 2 ms width pulses with a pulse separation of 2 ms. In the last case, the pulse energy was set to 120 nJ that corresponds to a peak power of 60 mW (same as the power used under CW excitation). The thermal images show similar temperature distributions. In both cases, the thermal pattern is characterized by a remarkable thermal confinement inside the WG area. This unequivocally indicates that time modulation of the heat generation source has not effect on the spatial distribution of heat that it is mainly determined by the spatial confinement of pump radiation and the existence of thermal barriers (damage tracks). On the other hand, the magnitudes of the temperature increments are quite different. Indeed, time modulation of pump beam leads to a significant reduction in the maximum temperature increment inside the WG from 113 °C down to 60 °C. Figure 5 demonstrates the advantages of using modulated pump radiations for the minimization of undesirable thermal effects in integrated optical devices.

3.3 Numerical simulation

In order to corroborate the correctness of our measurements and the validity of our conclusions, numerical simulations of the thermal diffusion equation have been carried out by applying a finite difference approach. Thermal and spectroscopic properties assumed in our calculations were extracted from previous works describing Erbium and Ytterbium codoped phosphate glasses [31,32].

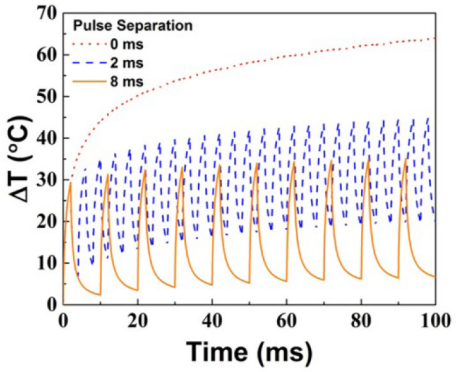

Fig. 6. Simulated time evolution of pump-induced temperature increment inside the WG for three different time configuration of the 980-nm "pump" radiation. The pulse separations are 0 ms (i.e. CW laser, dot), 2 ms (dash), and 8 ms (solid), from top to bottom, respectively.

Figure 6 shows the time evolution of the temperature inside the WG for three different time configuration of the 980-nm pump radiation. The dot line in Fig. 6 shows the calculated temperature when the pump beam was assumed to be a CW beam with a constant pump

Optics EXPRESS

power of 60 mW. Saturation is achieved when the heating rate caused by the absorption of pump radiation is equal to the heat dissipation due to temperature differences between environment and phosphate glass. When the pump beam was constituted by 2 ms pulses with a pulse separation of 2 ms, the time evolution of intra-waveguide temperature increment is shown in Fig. 6 (dash line). In this case, temperature increases during the laser pulse and relaxes during the time interval between pulses. Particularly, simulations reveal that complete thermal relaxation does not occur between consecutive pulses and thus heat accumulation takes place. As a consequence, WG temperature increases, on average, with time. It should be noted that the partial thermal relaxation between pulse leads to an average WG temperature smaller than that achieved under CW excitation. Finally, the solid curve in Fig. 6 shows the time evolution of WG temperature when the pulse separation was set to 8 ms that is larger than the characteristic thermal relaxation time. Again, WG temperature increases during the pump pulse but, at variance with previous cases, almost complete thermal relaxation occurs between pulses. In this case thermal accumulation between consecutive pulses is almost negligible and, consequently, the average WG temperature increment is almost negligible. The average temperature increment normalized to the temperature increment induced under CW excitation (T_{norm}) as a function of the time distance between pulses extracted from numerical calculations (triangles) has been included together with experimental data (solid circles) in Fig. 5(c). As can be observed, an excellent agreement between experimental data and numerical calculations has been obtained revealing the correctness of our calculations as well as the role played by thermal accumulation in the observed minimization of thermal loading when using time-modulated pump radiations.

4. Summary

In summary, we have demonstrated how the high thermal sensitivity of the two-photon excited luminescence of Erbium ions, in combination with high resolution multiphoton fluorescence imaging, constitutes an accurate, reliable and flexible three dimensional, contact-free technique for thermal imaging of photonic devices. In particular, we have provided high resolution 3D thermal images of 980-nm laser pumped ULI channel waveguide in an Erbium and Ytterbium codoped phosphate glass. Thermal images have revealed that in these structures laser induced thermal loading cannot be neglected at all. Temperature increments at waveguide's volume as large as 200 °C have been found for moderate pump powers of 120 mW. Furthermore, thermal images have also revealed a strong confinement of the pump induced thermal load at the waveguide's volume revealing the thermal impedance caused by the damage tracks that simultaneously behave as thermal and optical barriers.

Thermal images have also indicated that such relevant pump induced intra-waveguide thermal loading can be substantially reduced by time modulation of the pump beam. Experimental and numerical simulations have concluded that intra-waveguide thermal relaxation times are in the millisecond time scale in such a way that heat accumulation can be minimized by using pulse pump beams with time separation between pulses of few milliseconds.

This work introduces to the scientific community a high resolution, flexible, simple and versatile tool for the acquisition of 3D high resolution and time resolved thermal images of active photonic devices that would be essential for the complete understanding of their optical performance as well as for the optimization of their optical performance.

Funding

Ministerio de Economía y Competitividad of Spain (MINECO) (FIS2013-44174-P, MAT2013-47395-C4-1-R); National Natural Science Foundation of China (NSFC) (11274203).

Optics EXPRESS

Acknowledgments

Ruiyun He thanks the support of the China Scholarship Council.